## High-temperature low pressure chemical vapor deposition of β-Ga<sub>2</sub>O<sub>3</sub>

Yuxuan Zhang<sup>1\*</sup>, Zixuan Feng<sup>1\*</sup>, Md Rezaul Karim<sup>1</sup>, Hongping Zhao<sup>1, 2, a)</sup>

<sup>1</sup>Department of Electrical and Computer Engineering, The Ohio State University, Columbus, OH 43210. USA

<sup>2</sup>Department of Materials Science and Engineering, The Ohio State University, Columbus, OH 43210, USA

a) Electronic mail: <u>zhao.2592@osu.edu</u>

\*Equally contributed first authorship

Recent advancements in β-Ga<sub>2</sub>O<sub>3</sub> materials growth and device developments are briefly reviewed with the focus on low pressure chemical vapor deposition (LPCVD) of β-Ga<sub>2</sub>O<sub>3</sub>. The growths of  $\beta$ -Ga<sub>2</sub>O<sub>3</sub> films on off-axis c-sapphire and (010)  $\beta$ -Ga<sub>2</sub>O<sub>3</sub> substrates are performed via high-temperature LPCVD (HT-LPCVD) with growth temperatures ranging between 950 and 1050 °C. The effects of HT-LPCVD growth conditions on material properties are comprehensively studied. With relatively higher growth temperatures, increased O<sub>2</sub> flow rate is required to maintain β-Ga<sub>2</sub>O<sub>3</sub> crystalline quality with high electron mobility. The growth rate of HT-LPCVD β-Ga<sub>2</sub>O<sub>3</sub> film scales with the increase of growth temperature and O<sub>2</sub> flow rate. The film growth rate is strongly related to the sapphire substrate off-axis angle, which determines the preferred nucleation sites from the step edges. The transport properties of samples grown on substrates with different off-axis angles are compared. The optimized growth temperature for obtaining films with high electron mobility varies with the off-axis angle. From this comprehensive study, high quality β-Ga<sub>2</sub>O<sub>3</sub> films grown on c-sapphire are achieved with room temperature mobility of 126 cm<sup>2</sup>/Vs (6° off-axis c-sapphire), 116 cm<sup>2</sup>/Vs (8° offaxis c-sapphire) and 119 cm<sup>2</sup>/Vs ( $10^{\circ}$  off-axis c-sapphire) at carrier concentrations of mid- $10^{16}$  cm<sup>-3</sup>.  $\beta$ -Ga<sub>2</sub>O<sub>3</sub> LPCVD homoepitaxy optimized at elevated growth temperature is performed on Fe-doped semi-insulating (010) Ga<sub>2</sub>O<sub>3</sub> substrates. With controllable Si doping, record-high room temperature mobilities of 156 cm<sup>2</sup>/Vs (150 cm<sup>2</sup>/Vs) are achieved with doping concentrations of  $3\times10^{16}$  cm<sup>-3</sup> ( $1.5\times10^{17}$  cm<sup>-3</sup>) at a growth temperature of 1050 °C. Secondary ion mass spectroscopy analysis shows more than an order of magnitude reduction of C and H impurity incorporation with increased growth temperature. Results from this work demonstrate that HT-LPCVD growth is a promising method to produce high-quality  $\beta$ -Ga<sub>2</sub>O<sub>3</sub> films on both off-axis c-sapphire and native Ga<sub>2</sub>O<sub>3</sub> substrates with fast growth rate and superior transport properties critical for high power device applications.

### I. Introduction to gallium oxide materials and devices

Gallium oxide (Ga<sub>2</sub>O<sub>3</sub>) has attracted significant interests as an ultra-wide bandgap (UWBG) semiconductor material with an energy bandgap of 4.5 - 4.9 eV, which is larger than traditional WBG semiconductors such as SiC (3.2 eV) and GaN (3.4 eV). Among all Ga<sub>2</sub>O<sub>3</sub> phases that have been identified [1], the monoclinic β phase represents the most stable crystal structure with two different Ga sites and three different O sites in a unit cell. As a result of its large bandgap, β-Ga<sub>2</sub>O<sub>3</sub> is estimated to possess a high critical field strength of 8 MV/cm, which is 2.5 - 3.5 times that of SiC (2.5 MV/cm), and GaN (3.3 MV/cm) [2]. Besides, its optical transparency in the deep ultraviolet (DUV) wavelength regime enables potential application for DUV optoelectronic devices, such as solar-blind photodetectors [3, 4]. β-Ga<sub>2</sub>O<sub>3</sub> has been demonstrated with n-type doping with shallow

donors, including silicon (Si), germanium (Ge), and tin (Sn) [5-12]. Particularly, Si has been demonstrated as an effective shallow donor in chemical vapor deposition (CVD) based growth methods with a wide doping range from 10<sup>15</sup> to 10<sup>20</sup> cm<sup>-3</sup>, essential for electronic and optoelectronic device applications. On the other hand, p-type doping in β-Ga<sub>2</sub>O<sub>3</sub> is considered very challenging based on first-principle density functional theory (DFT) calculations, which predicted deep acceptors and self-trapping hole effects due to the formation of localized polarons [13, 14]. One key advantage for β-Ga<sub>2</sub>O<sub>3</sub> epitaxy is from the availability of high quality native Ga<sub>2</sub>O<sub>3</sub> substrates synthesized via scalable melt growth techniques, such as floating zone (FZ) [15], edge defined film-fed growth (EFG) [12, 16], and Czochralski [17, 18] methods. Currently, 4" Ga<sub>2</sub>O<sub>3</sub> substrates are commercially available at Novel Crystal Technologies, and 6" substrates have been demonstrated.

In recent years, tremendous progress has been made for  $\beta$ -Ga<sub>2</sub>O<sub>3</sub> based electronic device demonstrations. Since the early demonstration of lateral transistor with 39 mA/mm current capacity by Higashiwaki et al., [19],  $\beta$ -Ga<sub>2</sub>O<sub>3</sub> has shown its potential and feasibility in power electronic applications. With continuous advancements in materials growth, device structure design, dielectric selection, and contact optimization, device performance has shown promising improvements over the years. Thus far, 3.8 MV/cm gate-to-drain electric field has been exhibited in  $\beta$ -Ga<sub>2</sub>O<sub>3</sub> metal-oxide-semiconductor field-effect transistor (MOSFET) [20], which surpassed the theoretical limits of GaN and SiC based devices.

Vertical Schottky barrier diodes grown by low-pressure chemical vapor deposition (LPCVD) were demonstrated with a breakdown field of 4.2 MV/cm in the

center and 5.8 MV/cm at the edge of the field plate structure [21]. A vertical Schottky diode with combined guard ring and field-plate structure, grown by halide vapor phase epitaxy (HVPE), was reported to sustain a breakdown voltage of 1.43 kV with an onresistance of 4.7 m $\Omega$ ·cm<sup>2</sup> [22]. Most recently, a vertical fin-structured transistor with normally-off characteristics has been demonstrated, with breakdown voltage of 1.6 kV and drain current density of 600 A/cm<sup>2</sup> [23]. A similar fin-structured SBD was reported with 2.89 kV breakdown voltage using a refined field-plate design [24]. The measured specific on-resistance ( $R_{on,sp}$ ) was estimated at 8.2 m $\Omega$ ·cm<sup>2</sup> and effective Baliga's figure-of-merit (BFOM) of 0.8 (0.95) GW/cm<sup>2</sup> under DC (pulsed) condition. These successful demonstrations of  $\beta$ -Ga<sub>2</sub>O<sub>3</sub> based devices with promising device characteristics prove  $\beta$ -Ga<sub>2</sub>O<sub>3</sub> a potential UWBG semiconductor for next-generation power electronics. Nevertheless, the continuous advancement of  $\beta$ -Ga<sub>2</sub>O<sub>3</sub> based device performance requires the development of high crystalline quality materials with low background doping and controllable doping level in a wide range.

Several growth methods have been investigated for developing β-Ga<sub>2</sub>O<sub>3</sub> thin film epitaxy including molecular beam epitaxy (MBE) [8, 11, 25-30], HVPE [5, 31-32], metal-organic chemical vapor deposition (MOCVD) [6-7, 34-36], and LPCVD [10, 38-41]. For MBE growth, two oxygen sources including oxygen plasma and ozone have been used and the former is a more common O precursor [8, 25]. Si, Sn, and Ge are investigated as shallow donors for MBE β-Ga<sub>2</sub>O<sub>3</sub> [8, 11, 26]. Room temperature (RT) mobility reported on MBE β-Ga<sub>2</sub>O<sub>3</sub> typically ranges between 80-140 cm<sup>2</sup>/Vs with Sn, Ge as the n-type dopants [8, 11]. The growth rate of MBE β-Ga<sub>2</sub>O<sub>3</sub> is generally slow in the range of 50~200 nm/hr on (010) Ga<sub>2</sub>O<sub>3</sub> substrate. MBE growths of β-Ga<sub>2</sub>O<sub>3</sub> along other

crystal orientations such as (001) and (100) have shown even lower growth rates due to significant adatom surface desorption. [27]. Recently, a metal-oxide catalyzed epitaxy (MOCATAXY, or metal exchange catalyzed, MEXCAT) was proposed to widen the MBE growth window and increase Al incorporation in MBE AlGaO growth [28-30]. Based on the metal-exchange catalytic effect, the incorporation of indium flux at the growth interface could greatly reduce the surface desorption of sub-oxides and thus lead to the increase of growth rates of β-Ga<sub>2</sub>O<sub>3</sub> [28].

HVPE has been demonstrated to produce high-quality  $\beta$ -Ga<sub>2</sub>O<sub>3</sub> films with fast growth rates (~5 - 250 μm/hr) [31, 32]. Gallium chloride (GaCl) and oxygen (O<sub>2</sub>) are used as precursors, with growth temperature typically at ~ 1000°C [5]. Silicon tetrachloride (SiCl<sub>4</sub>) is commonly used as n-type dopant source. HVPE growth of β-Ga<sub>2</sub>O<sub>3</sub> provides the feasibility to obtain a thick drift layer needed for high power vertical devices. However, the fast growth rates in HVPE β-Ga<sub>2</sub>O<sub>3</sub> also cause rough surface morphologies which often require additional mechanical-chemical polishing prior device fabrication [32]. The use of Cl based precursor and its incorporation in the grown film may create defect states causing charge compensation [33]. For HVPE grown β-Ga<sub>2</sub>O<sub>3</sub>, the best measurable RT mobility is 149 cm<sup>2</sup>/Vs at a low charge density of 3×10<sup>15</sup> cm<sup>-3</sup> [5].

MOCVD growth of  $\beta$ -Ga<sub>2</sub>O<sub>3</sub> has been demonstrated with high crystalline quality and effective n-type doping in a wide doping range [6, 7, 35, 36]. Triethylgallium (TEGa) or Trimethylgallium (TMGa), high purity O<sub>2</sub> or H<sub>2</sub>O vapor have been used as precursors. Although both Si and Sn were demonstrated as shallow donors [7], Si is considered as a preferable dopant in MOCVD β-Ga<sub>2</sub>O<sub>3</sub>. Intentional Si-doped MOCVD grown β-Ga<sub>2</sub>O<sub>3</sub>

thin film on (010) Ga<sub>2</sub>O<sub>3</sub> substrate with record-high room temperature mobility of 184 cm<sup>2</sup>/Vs and low temperature peak mobility of 4984 cm<sup>2</sup>/Vs was demonstrated [6]. The extracted low compensation level at  $\sim 9.4 \times 10^{14}$  cm<sup>-3</sup> promises its controllable doping at low levels critical for high power electronics. Recently, record high low-temperature peak mobilities of 9500-11,000 cm<sup>2</sup>/Vs have been achieved from MOCVD growth of  $\beta$ -Ga<sub>2</sub>O<sub>3</sub> [36, 37]. These results indicate that MOCVD grown  $\beta$ -Ga<sub>2</sub>O<sub>3</sub> have high crystalline quality with high purity. Most recent demonstration of high quality (Al<sub>x</sub>Ga<sub>1-x</sub>)<sub>2</sub>O<sub>3</sub> films with high Al composition via MOCVD indicates its great potential for developing device-quality AlGaO thin films and AlGaO/GaO heterostructures for high-performance device applications [42, 43].

### II. LPCVD growth of β-Ga<sub>2</sub>O<sub>3</sub>

LPCVD represents a low-cost and scalable growth technique for β-Ga<sub>2</sub>O<sub>3</sub> thin films with good crystalline quality and controllable n-type doping. LPCVD of β-Ga<sub>2</sub>O<sub>3</sub> uses high-purity metallic Ga and oxygen as precursors, and growth pressure ranging between 1 Torr and 15 Torr. The metallic source contained in a crucible is placed in a horizontal growth chamber, which is heated up during the growth process. Substrates are placed downstream to the Ga precursors. A schematic of the LPCVD growth system is illustrated in Fig. 1. As the growth chamber heats up, Ga evaporates and first reacts with oxygen (O<sub>2</sub>) to form gas-phase sub-oxide Ga<sub>2</sub>O. Then it is carried to the downstream by carrier gas (Argon, Ar) and further reacts with O<sub>2</sub> to form Ga<sub>2</sub>O<sub>3</sub> on substrates. SiCl<sub>4</sub> is used as an n-type dopant precursor. The typical growth temperature for LPCVD Ga<sub>2</sub>O<sub>3</sub> ranges between 800 °C to 950 °C. The growth temperature, precursor flow rate, carrier gas flow rate, and chamber pressure are identified as critical growth parameters. In

addition, the similar growth technique has been demonstrated to grow high-quality In<sub>2</sub>O<sub>3</sub> films with fast growth rates on various substrates [45-47].

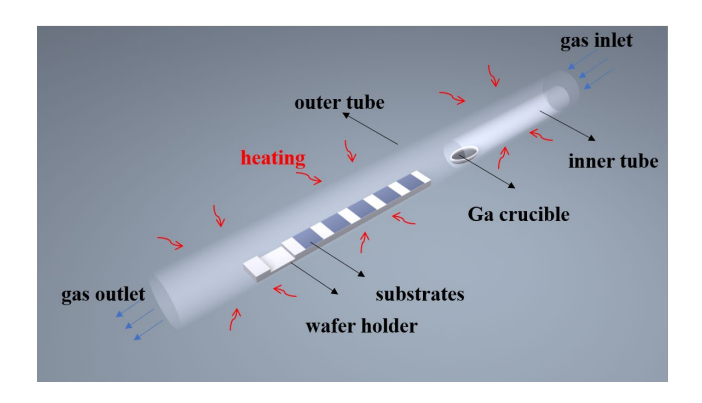


FIG. 1. Schematic view of an LPCVD Ga<sub>2</sub>O<sub>3</sub> system.

The LPCVD growth of  $\beta$ -Ga<sub>2</sub>O<sub>3</sub> was first explored on the c-plane sapphire substrates, with the proof of concept published in 2015 by Rafique et al. [38], followed with detail studies on crystallinity, doping and electron transport properties [40]. The heteroepitaxy on c-plane sapphire was found to be single  $\beta$ -phase Ga<sub>2</sub>O<sub>3</sub> with (-201) as the growth orientation under compressive strain. The full-width half-maximum (FWHM) of the X-ray diffraction (XRD) rocking curve (XRC) was ~ 1° for the (-201) peak. However, the electron backscatter diffraction (EBSD) [40] and XRD phi-scan revealed the existence of in-plane rotational domains in the film [10], which leads to the limited electron mobilities in as-grown films. To address this challenge, off-axis sapphire substrates were introduced to suppress the structural defects formed due to rotational domains. Results indicate that material crystalline quality was significantly improved with a narrower XRC FWHM (0.47°) and enhanced room temperature mobility (106 cm<sup>2</sup>/Vs) grown on 6° off-axis sapphire [10].

LPCVD homoepitaxy of  $\beta$ -Ga<sub>2</sub>O<sub>3</sub> was also demonstrated with unintentional doping [39] and Si doping [41] on (010) and (001) Ga<sub>2</sub>O<sub>3</sub> substrates. Room temperature electron Hall mobilities of 72 cm<sup>2</sup>/Vs and 42 cm<sup>2</sup>/Vs were measured on Si-doped (010) and (001)  $\beta$ -Ga<sub>2</sub>O<sub>3</sub>, with RMS surface roughness of 3 nm and 4 nm, respectively. The films show similar growth rates along different crystal growth orientation.

The dependence of LPCVD  $\beta$ -Ga<sub>2</sub>O<sub>3</sub> growth rate, doping concentration, and electron mobility on growth parameters were systematically studied [44]. By combining experiments and computational fluid dynamics (CFD) modelling, the study revealed that the oxygen flow rate, carrier gas Ar flow rate, growth temperature, chamber pressure, and distance between the source crucible and substrate can affect the film growth rate and material quality of LPCVD  $\beta$ -Ga<sub>2</sub>O<sub>3</sub>. The exponential decay of the film growth rate versus source-substrate distance revealed the gas phase reaction as a dominant chemical reaction in the growth chamber, other than the reactions on the hot chamber wall and substrates [44]. The CFD prediction of gas transport and the growth rate agreed well with the experimental observation, which provided insights of LPCVD  $\beta$ -Ga<sub>2</sub>O<sub>3</sub> growth mechanism and guidance on control of film growth rate and doping.

Significant progress has been made for developing LPCVD of  $\beta$ -Ga<sub>2</sub>O<sub>3</sub> in the past few years. Continuous efforts are still required to lower impurity levels (such as C, H) in the as-grown films and understand the sources of compensation which can limit both room temperature and low temperature transport properties. The rest of this paper focuses on the investigation of LPCVD  $\beta$ -Ga<sub>2</sub>O<sub>3</sub> thin films at higher growth temperature regime on both off-axis c-plane sapphire and (010)  $\beta$ -Ga<sub>2</sub>O<sub>3</sub> substrates. Comprehensive studies indicate the high temperature LPCVD (HT-LPCVD) growth can produce better quality  $\beta$ -

Ga<sub>2</sub>O<sub>3</sub> thin films with improved surface morphology, lower impurity concentrations, and superior transport properties.

## **III. HT-LPCVD: Experiment**

The β-Ga<sub>2</sub>O<sub>3</sub> films were grown via HT-LPCVD on c-plane sapphire substrates with off-axis angle ranging from 3.5° to 10° toward sapphire <11-20> ( $\Delta_a$ ), and Fe-doped semi-insulating (010) β-Ga<sub>2</sub>O<sub>3</sub> substrate. High purity metallic Ga (Alfa Aesar, 99.9999%) was placed in quartz crucible at the upstream of the substrates. High purity O<sub>2</sub> gas was used as precursor with flow rate ranging from 10 to 30 standard cubic centimeters per minute (sccm). Ar was used as a carrier gas with a fixed flow rate of 200 sccm. SiCl<sub>4</sub> was used as n-type dopant source. The growth temperature was varied between 900°C and 1050 °C, and growth pressure was fixed at 2 Torr. The surface morphology and cross-section of β-Ga<sub>2</sub>O<sub>3</sub> films were characterized by Helios Nanolab 600 field emission scanning electron microscopy (FESEM). The film thickness and hence the growth rate was estimated from the cross-sectional FESEM images. The surface morphology of samples grown on β-Ga<sub>2</sub>O<sub>3</sub> substrate was characterized by Bruker Icon 3 atomic force microscopy (AFM). Titanium/gold (Ti/Au) contacts were deposited on asgrown samples for carrier transport measurements. RT Hall mobilities were measured by Van-der-Pauw Hall configuration using the Ecopia HMS-3000 Hall effect system.

## IV. HT-LPCVD: Results and Discussions

## A. HT-LPCVD growth of $\beta$ -Ga<sub>2</sub>O<sub>3</sub> on off-axis c-sapphire ( $\Delta_a$ =6°) substrate

A series of experiments were carried out to investigate the effect of growth temperature and  $O_2$  flow rate on the growth of  $\beta$ -Ga<sub>2</sub>O<sub>3</sub> films on off-axis c-sapphire substrates with  $\Delta_a$ =6°. Four off-axis c-sapphire substrates ( $\Delta_a$ =6°) were placed at 4.5, 6.5, 14, and 16 cm downstream to the crucible, respectively. Film growth rates and RT transport properties were studied with various  $O_2$  flow rates (10, 15, 20, and 30 sccm, respectively) under different growth temperatures (900, 950, 1000 and 1050 °C, respectively). The SiCl<sub>4</sub> flow rate was fixed at 0.1 sccm.

Figure 2 plots the growth rate (Fig. 2(a)), Hall mobility (Fig. 2(b)), bulk (Fig. 3(c)) and sheet carrier concentration (Fig. 2(d)) under different growth temperatures with varied O<sub>2</sub> flow rates. As seen in Fig. 2(a), despite the growth conditions with different growth temperatures (900 -1050 °C) and O<sub>2</sub> flow rates (10-30 sccm), the β-Ga<sub>2</sub>O<sub>3</sub> film growth rates decrease with the increase of the substrate distance to crucible in all groups, which have also been observed in our previous studies on LPCVD β-Ga<sub>2</sub>O<sub>3</sub> and In<sub>2</sub>O<sub>3</sub> [44, 46]. The mechanism has been studied by a CFD model [44], that with the increase of distance from the sample to the crucible, the gas-phase reaction and reduction in the concentration of reaction species limit the growth rate, resulting in an exponential decay as a function of distance. It is also observed that with a simultaneous increase in growth temperature and O<sub>2</sub> flow rate, the film growth rate shows a significant increase. This is due to the stronger Ga evaporation from increased temperature. The increase of O<sub>2</sub> flow rate at higher growth temperature maintains Ga/O ratio in a similar range, which also results in faster growth rates.

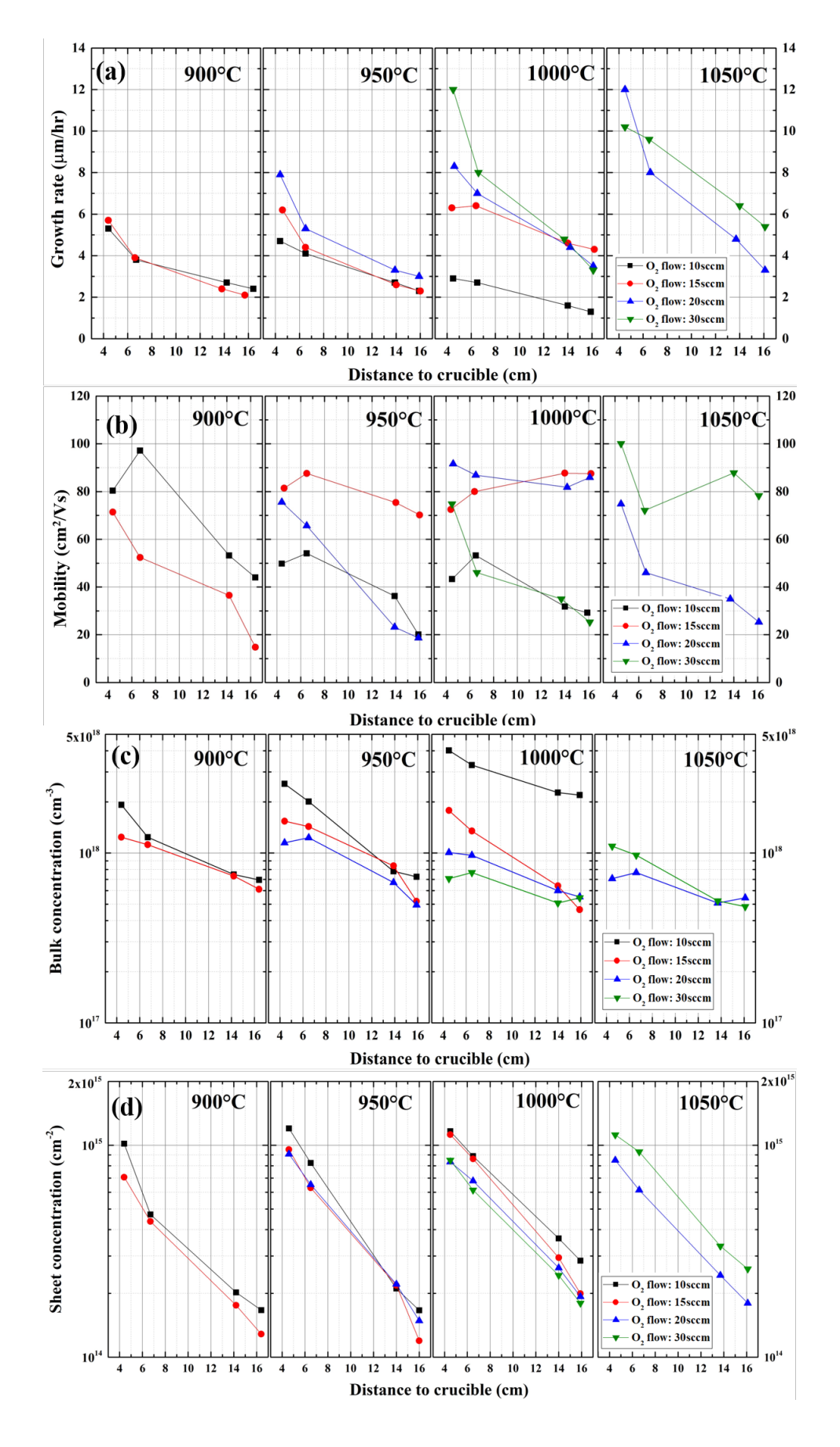


FIG. 2. LPCVD  $\beta$ -Ga<sub>2</sub>O<sub>3</sub> film (a) growth rate, (b) mobility (c) bulk concentration and (d) sheet concentration as a function of substrate distance to crucible at different growth temperatures and O<sub>2</sub> flow rates. Off-axis sapphire substrates with  $\Delta_a$ =6° were used. Ar flow rate was fixed at 200 sccm and SiCl<sub>4</sub> flow rate was fixed at 0.1 sccm.

As shown in Fig. 2(b), the combination of temperature and  $O_2$  flow rate has a significant influence on RT mobility of  $\beta$ -Ga<sub>2</sub>O<sub>3</sub>. For samples grown at 900 °C, higher mobilities were obtained with 10 sccm O<sub>2</sub> flow rate. As the temperature increased to 950 °C, films grown with 15 sccm O<sub>2</sub> flow rate show higher mobility values as compared to those grown with O<sub>2</sub> flow rate of 10 or 20 sccm. When the temperature was elevated to 1000 °C, samples grown with O<sub>2</sub> flow rate of 15 and 20 sccm exhibits higher mobilities, whereas tuning O<sub>2</sub> flow rate to either higher (30 sccm) or lower (10 sccm) resulted in lower mobilities. As for the growth temperature at 1050 °C, higher mobilities were obtained for samples grown with high O<sub>2</sub> flow rate at 30 sccm. The mapping of growth conditions revealed that simultaneous increase of both temperature and O<sub>2</sub> flow rate is required to obtain high mobility  $\beta$ -Ga<sub>2</sub>O<sub>3</sub> films. With a fixed growth temperature, there exists an optimal O<sub>2</sub> flow rate that leads to maximum electron mobilities. Considering the temperature dependence of Ga evaporation rate, this study indicates that the optimal Ga/O ratio is critical to achieving LPCVD  $\beta$ -Ga<sub>2</sub>O<sub>3</sub> films with high mobilities.

Figure 2(c) plots the bulk carrier concentration as a function of the substrate to crucible distance at different temperatures with varying O<sub>2</sub> flow rates. The overall trend shows that bulk concentration decreases with the increase of distance. The reduction of carrier concentration is likely due to the consumption of Si precursors as the distance of

downstream substrates increases. Equation (1) [48] formulates the incorporation rate of dopant atoms per unit volume  $(N_d)$  as a function of the growth rate  $(G_r)$ , sticking coefficient  $(S_d)$ , and dopant flux to substrate surface  $(J_d)$ .

$$N_d = J_d S_d \frac{1}{G_r} \tag{1}$$

With the same growth time of one hour, the sheet carrier concentration  $N^{2D} \propto N_d G_r$ , then Equation (1) can be rewritten as

$$N^{2D} \propto I_d S_d \tag{2}$$

Considering that the sticking coefficient is mainly related to temperature, pressure, and substrate surface condition in a CVD system [49, 50], it is reasonable to assume that  $S_d$  is a constant for each group with the same growth condition. Note that  $N^{2D}$  can be obtained from the bulk concentration  $N_d$  multiplies the corresponding film thickness. Therefore, one can obtain the decay trend of Si precursor as a function of the substrate to crucible distance from the  $N^{2D}$  vs. distance as shown in Fig. 2(d). From this study, the reduction of Si dopant incorporation in LPCVD  $\beta$ -Ga<sub>2</sub>O<sub>3</sub> films as a function of the substrate to crucible distance is mainly due to the consumption of SiCl<sub>4</sub> flowing from upstream along with the growth chamber. Note that both Ga and SiCl<sub>4</sub> can be consumed in the gas phase through reactions with O<sub>2</sub>, which limits the amount of precursors reaching the substrates. It suggests that as compared with Ga precursor, SiCl<sub>4</sub> has a faster consumption rate at the upstream of the growth chamber, resulting in the reduction of sheet charge as the substrates are placed further downstream.

## B. HT-LPCVD growth of β-Ga<sub>2</sub>O<sub>3</sub> on c-sapphire: effects of offaxis angles and growth conditions

To understand the effects of the substrate off-axis angle on surface morphology and transport properties with different growth conditions, a series of experiments were conducted. C-plane sapphire substrates with off-axis angle of  $\Delta_a$ =3.5°, 6°, 8°, and 10° were used in this study. Three growth conditions (Condition I, II, and III) were selected as listed in Table 1.

TABLE I. LPCVD optimal growth conditions of  $\beta$ -Ga<sub>2</sub>O<sub>3</sub> with different temperatures and O<sub>2</sub> flow rates.

Growth	Growth temperature	O <sub>2</sub> flow rate	Ar flow rate
condition	(°C)	(sccm)	(sccm)
I	950	15	
П	1000	20	200
III	1050	30	

For each case with a specific temperature, the O<sub>2</sub> flow rate was selected based on the findings in Section IV.A that the optimal O<sub>2</sub> flow rate increases as growth temperature increases. The SiCl<sub>4</sub> flow rate was varied between 0.0025 and 0.01 sccm to control the doping concentrations.

For each growth condition, six substrates were placed at different positions of the downstream of Ga crucible, with a specific distance of 2, 3, 4, 5, 6, and 7 cm (Sample #1 to #6), respectively. The sample surface morphology, film growth rate, and room temperature mobility values were compared. Figure 3 compares the surface morphologies of each Sample #2 grown under different growth conditions with various off-axis angles. From FESEM images shown in Fig. 3, the general trend exhibits the decease of step

width as the off-axis angle increases. As the growth temperature increases, the step boundaries become sharper, which is applicable for each case with different off-axis angles.

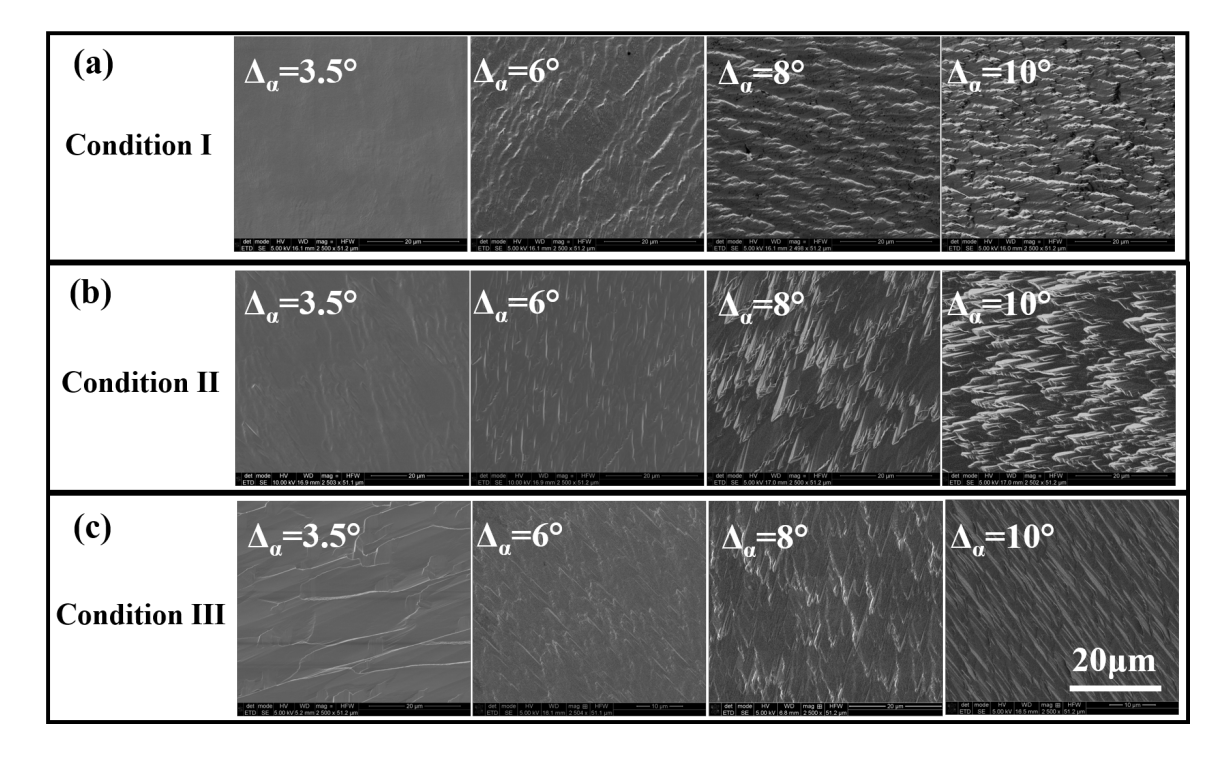


FIG. 3. FESEM images of surface morphologies of HT-LPCVD grown β-Ga<sub>2</sub>O<sub>3</sub> films on different off-axis c-plane sapphire substrates with growth (a) Condition I, (b) Condition II and (c) Condition III. All substrates were placed at the same position (3 cm downstream of Ga crucible) during the growth. Growth time was fixed for 1hr. The same scale bar was used for all images

The step edges of off-axis substrates act as preferential incorporation sites for Ga adatoms, resulting in the step flow growth along the off-axis direction. Note that stable step flow growth morphology can only be formed when the diffusion length of adatoms is comparable or larger than the width of terraces. On the contrary, random nucleation islands will form on the terraces before adatoms reaching the step edges. Since the terrace

width is inversely proportional to the tangent of the off-axis angle, with the same growth condition, Ga adatoms have a higher probability to reach step edges on substrates with a larger off-axis angle, thus forming uniform and stable step flow growth morphology. The diffusion length  $\lambda$  of adatoms can be expressed as  $\lambda = \sqrt{D\tau}$  where D represents the diffusion coefficient and  $\tau$  is the average lifetime of adatoms before being incorporated into crystals. Previous comprehensive study [51] on surface diffusion mechanisms formulated that  $D=D_0 \exp\left(-U_s/kT\right)$  and  $au= au_0 \exp\left(W_s/kT\right)$  where  $U_s$  is the activation energy of surface diffusion,  $W_s$  is the evaporation energy from the surface to the vapor, k is Boltzmann constant and T is temperature, respectively. Although this study indicated the trend that  $\lambda$  decreases monotonically with an increase of temperature, an opposite trend have been observed from several experimental studies [50, 52, 53]. Furthermore, Monte-Carlo simulation study [54] revealed that when growth temperature is lower than a critical temperature, surface diffusion length could increase with temperature. In our study, for films grown on substrates with the same off-axis angle, higher growth temperature leads to longer adatom diffusion length, therefore more uniform and continuous growths were observed.

Figure 4 plots the growth rate of  $\beta$ -Ga<sub>2</sub>O<sub>3</sub> films as a function of substrate distance to crucible with a fixed growth temperature of 1050 °C and O<sub>2</sub> flow rate of 30 sccm (Condition III).

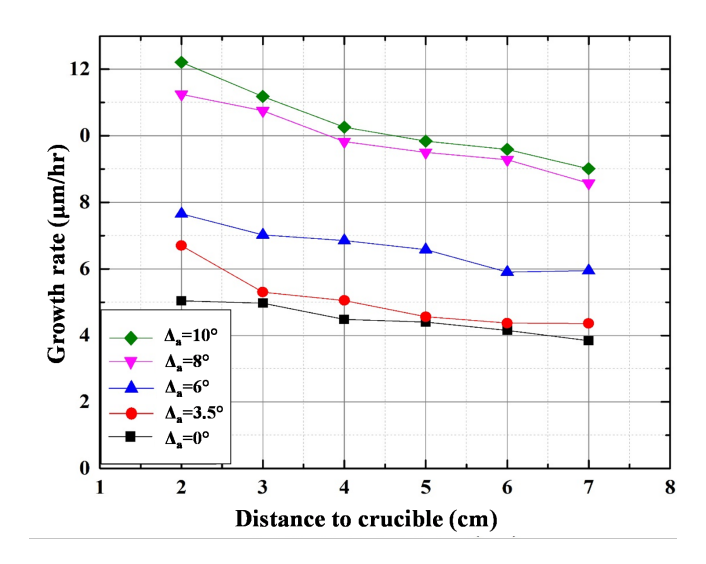


FIG. 4. HT-LPCVD  $\beta$ -Ga<sub>2</sub>O<sub>3</sub> film growth rate as a function of substrate distance to Ga crucible on sapphire substrates with off-axis angle  $\Delta_a$ =0°, 3.5°, 6°, 8°, and 10°. Growth temperature was set at 1050 °C with O<sub>2</sub> flow rate of 30 sccm (Condition III). All film thicknesses were obtained by FESEM cross-sectional imaging.

Regular c-plane sapphire ( $\Delta_a$ =0°) and off-axis sapphire substrates with off-axis angle of  $\Delta_a$ =3.5°, 6°, 8°, and 10° were used. Similar to the trend shown in Fig. 2(a), with the same off-axis angle, the film growth rate decreases as the substrate distance to crucible increases. This can be explained by the precursor consumption and gas phase reaction. For samples with different off-axis angles but the same distance to the crucible, the growth rate increases monotonically as the off-axis angle increases. Similar effects of off-axis angle on the growth rate have been observed in CVD-grown diamond [55]. The increase of off-axis angle reduces the terrace width, which in turn increases the density of step edges, providing more incorporation sites for adatoms and resulting in faster growth rates. Therefore, growth temperature and substrate off-axis angle are considered as two dominant parameters that can determine film surface morphology and growth rate.

# C. HT-LPCVD growth of β-Ga<sub>2</sub>O<sub>3</sub> on off-axis sapphire: transport properties

For electronic power device applications, high mobility and a wide range of controllable doping are essential that determine device performance. Here, the effects of off-axis angle and growth temperature on transport properties were compared and discussed. RT transport properties of LPCVD  $\beta$ -Ga<sub>2</sub>O<sub>3</sub> films grown on off-axis sapphire substrates under conditions listed in Table I were measured by van der Pauw method. The distance of substrates from Ga crucible and SiCl<sub>4</sub> flow rate were varied to obtain samples with different doping concentrations. Electron mobilities as a function of carrier concentration for films grown on various off-axis substrates were plotted separately as shown in Fig. 5. For each chart, the data include those grown under different conditions with a range of carrier concentration between  $10^{16}$  and  $10^{17}$  cm<sup>-3</sup>.

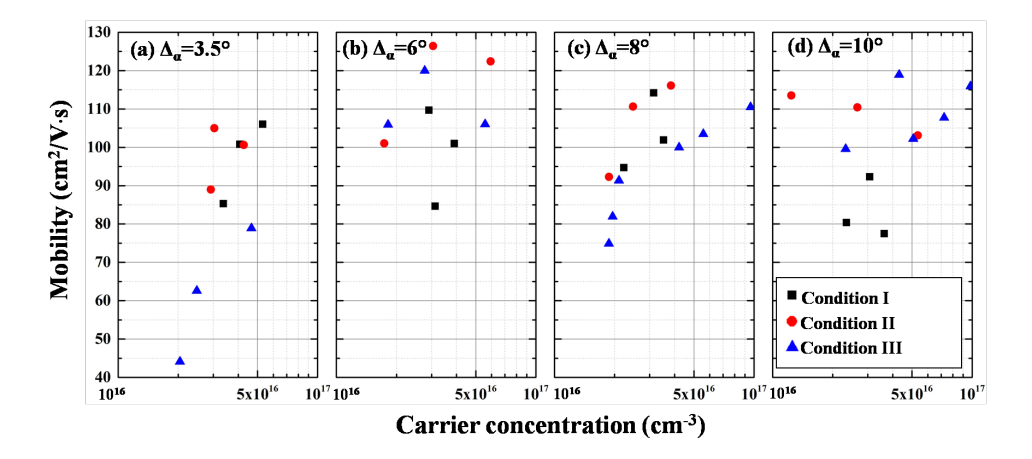


FIG. 5. Hall mobility vs. carrier concentration of HT-LPCVD  $\beta$ -Ga<sub>2</sub>O<sub>3</sub> films grown on off-axis sapphire substrates with (a)  $\Delta_a$ =3.5°, (b)  $\Delta_a$ =6°, (c)  $\Delta_a$ =8° and (d)  $\Delta_a$ =10° under growth Condition I, II and III.

From Fig. 5, high mobility values (>100 cm<sup>2</sup>/Vs) can be obtained in all four cases. However, there exists a strong correlation between mobilities and growth temperatures for films grown on different off-axis angles. For the case of  $\Delta_a$ =3.5°, relatively low growth temperatures (Condition I and II) can produce films with high mobilities. For example, mobility values of 106 cm<sup>2</sup>/Vs (Condition I) and 105 cm<sup>2</sup>/Vs (Condition II) were obtained as compared to those (< 80 cm<sup>2</sup>/Vs) grown with Condition III. For the cases of  $\Delta_a = 6^{\circ}$  and  $8^{\circ}$ , high mobility values were achieved at relatively higher growth temperatures. For the  $\Delta_a$ =6° group, mobility values over 110 cm<sup>2</sup>/Vs were achieved with Condition II (126 cm<sup>2</sup>/Vs, 122 cm<sup>2</sup>/Vs) and Condition III (120 cm<sup>2</sup>/Vs). For the  $\Delta_a$ =8° group, mobility values over 110 cm<sup>2</sup>/Vs were achieved under all growth conditions: Condition I (114 cm<sup>2</sup>/Vs), Condition II (116 cm<sup>2</sup>/Vs) and Condition III (111 cm<sup>2</sup>/Vs). With the further increase of  $\Delta_a$  to 10°, mobility values of samples grown at relatively low temperature (Condition I) decreased to 92 cm<sup>2</sup>/Vs, 81 cm<sup>2</sup>/Vs, and 78 cm<sup>2</sup>/Vs, while the values over 110 cm<sup>2</sup>/Vs were still achievable for Condition II (115 cm<sup>2</sup>/Vs) and III (119 cm<sup>2</sup>/Vs and 116 cm<sup>2</sup>/Vs). This study indicates that higher growth temperature is required for samples grown on substrates with larger off-axis angles to obtain optimal transport properties.

## D. HT-LPCVD growth of β-Ga<sub>2</sub>O<sub>3</sub> on (010) β-Ga<sub>2</sub>O<sub>3</sub> substrates

HT-LPCVD homoepitaxy of  $\beta$ -Ga<sub>2</sub>O<sub>3</sub> on semi-insulating Fe-doped (010)  $\beta$ -Ga<sub>2</sub>O<sub>3</sub> substrates were performed. The three growth conditions listed in Table I were used. The FESEM images of the surface morphologies of films grown at Condition I, II, and III, and the AFM image of the sample grown at Condition III are shown in Fig. 6.

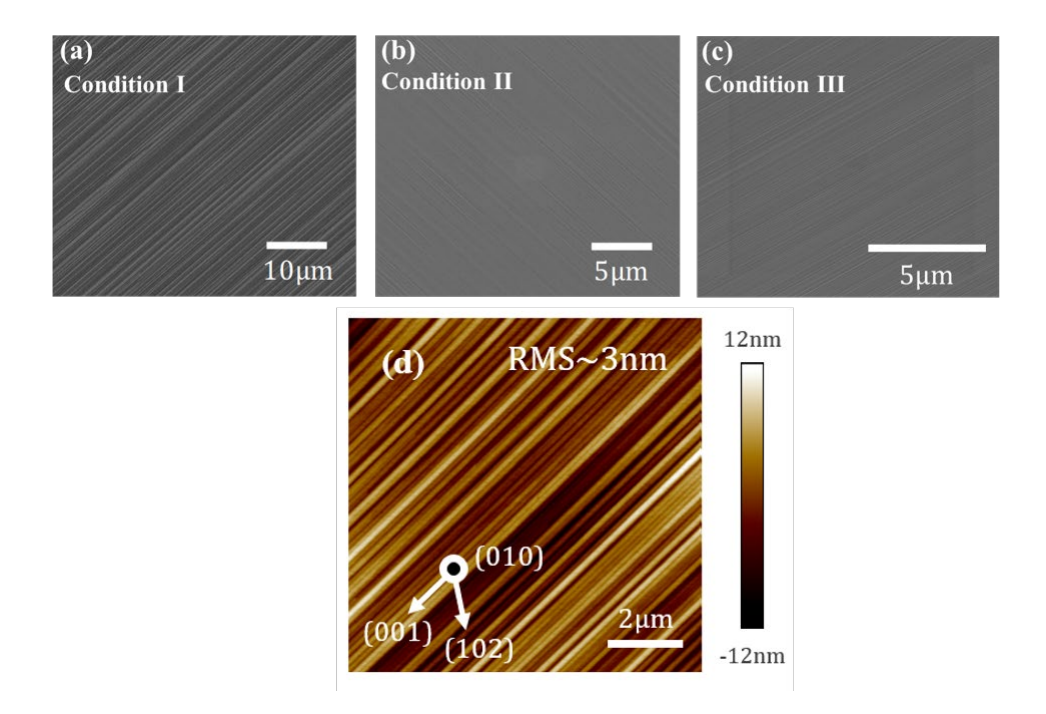


FIG. 6. FESEM images of HT-LPCVD β-Ga<sub>2</sub>O<sub>3</sub> samples grown with (a) Condition I (b) Condition II and (c) Condition III. (d) AFM image of β-Ga<sub>2</sub>O<sub>3</sub> film grown with Condition III. Detail growth conditions are listed in Table I.

As the growth temperature increased, the size of elongated features reduced which leads to smooth surface morphologies. AFM image of the sample grown at Condition III reveals a surface roughness RMS~3 nm, exhibiting improvement as compared with previous samples (RMS > 4 nm) grown with lower growth temperatures [41].

To evaluate the impurity levels in HT-LPCVD  $\beta$ -Ga<sub>2</sub>O<sub>3</sub>, quantitative SIMS was performed for the sample grown on Fe-doped (010) Ga<sub>2</sub>O<sub>3</sub> substrate at 1050 °C with 30 sccm O<sub>2</sub> flow rate (Condition III) for one hour. The SiCl<sub>4</sub> flow rate was set at 0.005 sccm. Depth profiles of Si, C, H, Fe, Cl and Ca were probed for 6  $\mu$ m from the top surface of the grown film, as shown in Fig. 7. The detection limit (DL) for each element is marked as dash lines in Fig. 7: Si (1×10<sup>15</sup> cm<sup>-3</sup>), C (2×10<sup>16</sup> cm<sup>-3</sup>), H (2×10<sup>16</sup> cm<sup>-3</sup>), Fe (5×10<sup>14</sup> cm<sup>-3</sup>)

³), Cl ( $5 \times 10^{14}$  cm<sup>-3</sup>), and Ca ( $2 \times 10^{13}$  cm<sup>-3</sup>). The Si concentration from SIMS measurement was at  $\sim 2 \times 10^{17}$  cm<sup>-3</sup>, which agrees well with the RT Hall measurement ( $\mu$ =149.6 cm<sup>2</sup>/Vs, n=1.5×10<sup>17</sup> cm<sup>-3</sup>), indicating that Si is the shallow donor that contributes to the conductivity.

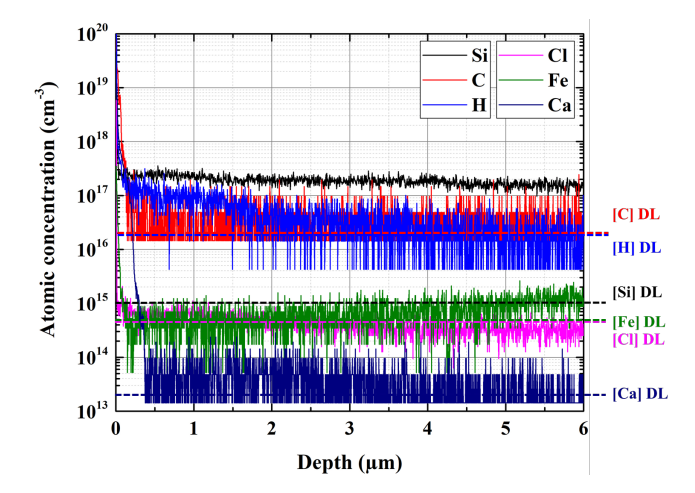


FIG. 7. SIMS depth profiles of HT-LPCVD homoepitaxial  $\beta$ -Ga<sub>2</sub>O<sub>3</sub> film grown on Fedoped (010) substrate with Condition III. Element detection limit (DL): Si:  $1 \times 10^{15}$  cm<sup>-3</sup>; C:  $2 \times 10^{16}$  cm<sup>-3</sup>; H:  $2 \times 10^{16}$  cm<sup>-3</sup>; Fe:  $5 \times 10^{14}$  cm<sup>-3</sup>; C1:  $5 \times 10^{14}$  cm<sup>-3</sup>; Ca:  $2 \times 10^{13}$  cm<sup>-3</sup>. The DL of each element is marked with dash lines.

C and H are considered as two common impurities in many compound semiconductors. The existence of these two impurities was observed in our previous report on LPCVD grown  $\beta$ -Ga<sub>2</sub>O<sub>3</sub> [41]. The origin of these impurities can be from the growth environment, precursors, as well as instrument components such as quartz tube. The quantitative SIMS results show that both elements were below the detection limit. C and H concentration in HT-LPCVD grown sample represent more than one order of reduction as compared to those grown with the same method but at lower temperature of 900 °C [41]. SiCl<sub>4</sub> was considered as the potential source of Cl incorporation. However,

SIMS shows that Cl concentration is below the detection limit, indicating the feasibility of using SiCl<sub>4</sub> as doping precursor in LPCVD  $\beta$ -Ga<sub>2</sub>O<sub>3</sub>. In addition, Ca is also below the detection limit. Regarding the Fe impurity, its concentration is below the detection limit in the top ~3  $\mu$ m film, while the impurity level shows a gradual increase as it approaches the growth interface due to Fe diffusion from substrate or surface riding effect.

The transport properties of homoepitaxy  $\beta$ -Ga<sub>2</sub>O<sub>3</sub> films grown under Condition III were studied. The SiCl<sub>4</sub> flow rate was varied to obtain different doping concentrations. Relatively high RT mobility values of 156 cm<sup>2</sup>/Vs and 150 cm<sup>2</sup>/Vs were achieved at doping concentrations of ~3×10<sup>16</sup> cm<sup>-3</sup> and ~ 1.5×10<sup>17</sup> cm<sup>-3</sup>, respectively. Figure 8 compares the RT mobility values as a function of carrier concentration of hetero- and homo-epitaxial HT-LPCVD  $\beta$ -Ga<sub>2</sub>O<sub>3</sub> films with mobility values obtained from conventional LPCVD growth conditions [39, 41], as well as data reported from other growth methods (MBE, MOCVD, and HVPE).

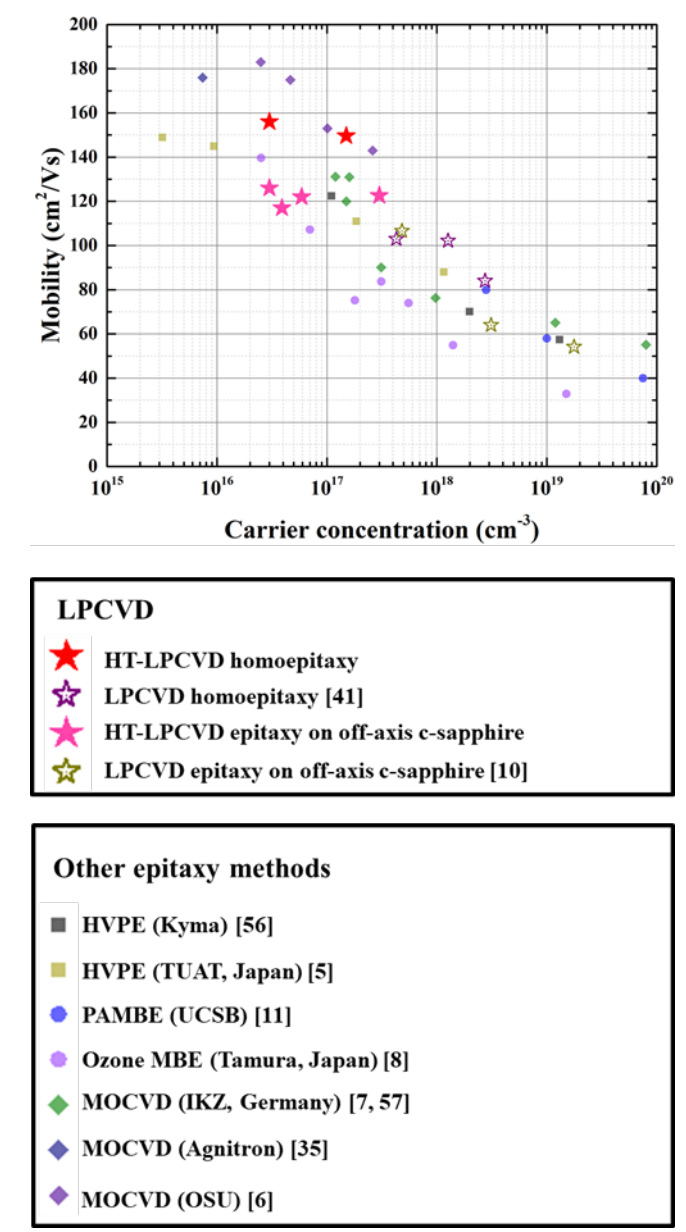


FIG. 8. Summary of mobility vs. carrier concentration of  $\beta$ -Ga<sub>2</sub>O<sub>3</sub> films grown by different growth methods. Mobility values of HT-LPCVD grown films are compared with those grown by lower temperature LPCVD conditions.

Using HT-LPCVD growth technique, β-Ga<sub>2</sub>O<sub>3</sub> mobility values were significantly improved for both hetero-epi and homo-epi films. The RT mobility values of HT-LPCVD

 $\beta$ -Ga<sub>2</sub>O<sub>3</sub> grown on (010) Ga<sub>2</sub>O<sub>3</sub> are among the best reported results. The superior RT transport properties of both hetero- and homo-epitaxial HT-LPCVD  $\beta$ -Ga<sub>2</sub>O<sub>3</sub> exhibit promising potential of LPCVD as a low cost and scalable growth method to grow high-quality  $\beta$ -Ga<sub>2</sub>O<sub>3</sub> films for device applications.

## V. Conclusion

In conclusion, HT-LPCVD growth of β-Ga<sub>2</sub>O<sub>3</sub> on both off-axis c-plane sapphire and (010) Ga<sub>2</sub>O<sub>3</sub> substrates was comprehensively studied. Effects of growth temperature, O<sub>2</sub> flow rate, and substrate off-axis angle on material properties were mapped. Studies show that there exist optimal Ga/O ratios at different growth temperatures. At relatively high growth temperature regime, O<sub>2</sub> flow rate is required to increase in order to obtain better mobility. β-Ga<sub>2</sub>O<sub>3</sub> film growth rate, surface morphology, and transport properties are significantly affected by substrate off-axis angles. Using HT-LPCVD growth conditions, record-high RT mobility for heteroepitaxy β-Ga<sub>2</sub>O<sub>3</sub> of 126 cm<sup>2</sup>/Vs, 116 cm<sup>2</sup>/Vs, and 119 cm<sup>2</sup>/Vs were obtained for films grown on 6°, 8°, and 10° off-axis sapphire substrates, respectively. HT-LPCVD growth of β-Ga<sub>2</sub>O<sub>3</sub> on native substrate also leads to better surface morphology with reduced roughness, and significant reduction of impurities incorporation such as C and H. Record high RT mobility of 156 cm<sup>2</sup>/Vs and 150 cm<sup>2</sup>/Vs were achieved at doping concentrations of  $\sim 3 \times 10^{16}$  cm<sup>-3</sup> and  $\sim 1.5 \times 10^{17}$  cm<sup>-3</sup>. respectively. The results from this work extend the growth window of LPCVD β-Ga<sub>2</sub>O<sub>3</sub> to higher growth temperature regime. The comprehensive mapping of the growth conditions on both off-axis c-sapphire and native Ga<sub>2</sub>O<sub>3</sub> substrates provides guidance for obtaining high quality films for device applications.

## **ACKNOWLEDGMENTS**

This project is partially funded by NSF (DMR-1755479) and Air Force Office of Scientific Research FA9550-18-1-0479 (AFOSR, Dr. Ali Sayir).

- <sup>1</sup>R. Roy, V.G. Hill and E.F. Osborn, J. Am. Chem. Soc. **74**, 719 (1952).
- <sup>2</sup>M. Higashiwaki, K. Sasaki, H. Murakami, Y. Kumagai, A. Koukitu, A. Kuramata, T. Masui, and S. Yamakoshi, Semicond. Sci. Tech. **31**, 034001 (2016).
- <sup>3</sup>M. Orita, H. Ohta, M. Hirano, and H. Hosono, Appl. Phys. Lett. 77, 4166 (2000).
- <sup>4</sup>T. Oshima, T. Okuno, N. Arai, N. Suzuki, S. Ohira, and S. Fujita, Appl. Phys. Express 1, 011202 (2008).
- <sup>5</sup>K. Goto, K. Konishi, H, Murakami, Y, Kumagai, B. Monemar, M. Higashiwaki, A. Kuramata, and S. Yamakoshi, Thin Solid Films **666**, 182 (2018).
- <sup>6</sup>Z. Feng, A F M A. U. Bhuiyan, M. R. Karim, and H. Zhao, Appl. Phys. Lett. **114**, 250601 (2019).
- <sup>7</sup>M. Baldini, M. Albrecht, A. Fiedler, K. Irmscher, R. Schewski, and G. Wagner, ECS J. Solid State Sci. Technol. **6**, Q3040 (2017).
- <sup>8</sup>K. Sasaki, A. Kuramata, T. Masui, E. G. Villora, K. Shimamura, and S.Yamakoshi, Appl. Phys. Express **5**, 035502 (2012).
- <sup>9</sup>A. T. Neal, S. Mou, S. Rafique, H. Zhao, E. Ahmadi, J. S. Speck, K. T. Stevens, J. D. Blevins, D. B. Thomson, N. Moser and K. D. Chabak, Appl. Phys. Lett. **113**, 062101 (2018).
- <sup>10</sup>S. Rafique, L. Han, A. T. Neal, S. Mou, J. Boeckl, and H. Zhao, Phys. Status Solidi A 215, 1700467 (2018).

- <sup>11</sup>E. Ahmadi, O. S. Koksaldi, S. W. Kaun, Y. Oshima, D. B. Short, U. K. Mishra, and J. S. Speck, Appl. Phys. Express 10, 041102 (2017).
- <sup>12</sup>A. Kuramata, K. Koshi, S. Watanabe, Y. Yamaoka, T. Masui, and S. Yamakoshi, Jpn. J. Appl. Phys. 55, 1202A2 (2016).
- <sup>13</sup>J. B. Varley, A. Janotti, C. Franchini, and C. G. Van de Walle, Phys. Rev. B **85**, 081109 (2012).
- <sup>14</sup>B. E. Kananen, N. C. Giles, L. E. Halliburton, G. K. Foundos, K. B. Chang, and K. T. Stevens, J. Appl. Phys. **122**, 215703 (2017).
- <sup>15</sup>Y. Tomm, J. M. Ko, A. Yoshikawa, and T. Fukuda, Sol. Energy Mater. Sol. Cells **66**, 369 (2001).
- <sup>16</sup>H. Aida, K. Nishiguchi, H. Takeda, N. Aota, K. Sunakawa, and Y. Yaguchi, Jpn. J. Appl. Phys. 47, 8506 (2008).
- <sup>17</sup>Y. Tomm, P. Reiche, D. Klimm, and T. Fukuda, J. Cryst. Growth **220**, 510 (2000).
- <sup>18</sup>Z. Galazka, K. Irmscher, R. Uecker, R. Bertram, M. Pietsch, A. Kwasniewski, M. Naumann, T. Schulz, R. Schewski, D. Klimm, and M. Bickermann, J. Cryst. Growth 404, 184 (2014).
- <sup>19</sup>M. Higashiwaki, K. Sasaki, T. Kamimura, M. H. Wong, D. Krishnamurthy, A. Kuramata, T. Masui, and S. Yamakoshi, Appl. Phys. Lett. 103, 123511 (2013).
- <sup>20</sup>A. J. Green, K. D. Chabak, E. R. Heller, R. C. Fitch, M. Baldini, A. Fiedler, K. Irmscher, G. Wagner, Z. Galazka, S. E. Tetlak, A. Crespo, K. Leedy, and G. H. Jessen, IEEE Electr. Device L. 37, 902 (2016)
- <sup>21</sup>C. Joishi, S. Rafique, Z. Xia, L. Han, S. Krishnamoorthy, Y. Zhang, S. Lodha, H. Zhao, and S. Rajan, Appl. Phys. Express 11, 031101 (2018).
- <sup>22</sup>C. H. Lin, Y. Yuda, M. H. Wong, M. Sato, N. Takekawa, K. Konishi, T. Watahiki, M. Yamamuka, H. Murakami, Y. Kumagai, and M. Higashiwaki, IEEE Electr. Device L. 40, 1487 (2019).

- <sup>23</sup>Z. Hu, K. Nomoto, W. Li, R. Jinno, T. Nakamura, D. Jena, and H. Xing, "1.6 kV Vertical Ga2O3 FinFETs With Source-Connected Field Plates and Normally-off Operation", ISPSD, 483, Shanghai, China (2019).
- <sup>24</sup>W. Li, K. Nomoto, Z. Hu, D. Jena, and H. G. Xing, IEEE Electr. Device L. **41**, 107 (2020).
- <sup>25</sup>M.-Y. Tsai, O. Bierwagen, M. E. White, and J. S. Speck, J. Vac. Sci. Technol. A **28**, 354 (2010).
- <sup>26</sup>K. Sasaki, M. Higashiwaki, A. Kuramata, T. Masui, and S. Yamakoshi, J. Cryst. Growth 392, 30 (2014).
- <sup>27</sup>T. Oshima, N. Arai, N. Suzuki, S. Ohira, and S. Fujita, Thin Solid Films **516**, 5768 (2008).
- <sup>28</sup>P. Mazzolini, A. Falkenstein, C. Wouters, R. Schewski, T. Markurt, Z. Galazka, M. Martin, M. Albrecht, and O. Bierwagen, APL Mater. 8, 011107 (2020).
- <sup>29</sup>P. Vogt, A. Mauze, F. Wu, B. Bonef and J. S. Speck, Appl. Phys. Express **11**, 115503 (2018).
- <sup>30</sup>P. Vogt, O. Brandt, H. Riechert, J. Lähnemann, and O. Bierwagen, Phys. Rev. Lett. **119**, 196001 (2017).
- <sup>31</sup>K. Nomura, K. Goto, R. Togashi, H. Murakami, Y. Kumagai, A. Kuramata, S. Yamakoshi, and A. Koukitu, J. Cryst. Growth 405, 19 (2014).
- <sup>32</sup>Y. Oshima, E.G. Villora, and K. Shimamura, J. Cryst. Growth 410, 53 (2015).
- <sup>33</sup>H. Murakami, K. Nomura, K. Goto, K. Sasaki, K. Kawara, Q.T. Thieu, R. Togashi, Y. Kumagai, M. Higashiwaki, A. Kuramata, S. Yamakoshi, B. Monemar, and A. Koukitu, Appl. Phys. Express 8, 015503 (2015).
- <sup>34</sup>G. Wagner, M. Baldini, D. Gogova, M. Schmidbauer, R. Schewski, M. Albrecht, Z. Galazka, D. Klimm, and R. Fornari, Phys. Status Solidi A 211, 27 (2014).
- <sup>35</sup>Y. Zhang, F. Alema, A. Mauze, O. S. Koksaldi, R. Miller, A. Osinsky, and J. S. Speck, APL Mater. 7, 022506 (2019).
- <sup>36</sup>F. Alema, Y. Zhang, A. Osinsky, N. Valente, A. Mauze, T. Itoh, and J. S. Speck, APL Mater. 7, 121110 (2019).

- <sup>37</sup>Z. Feng, A F M A. U. Bhuiyan, Z. Xia, W. Moore, Z. Chen, J. F. McGlone, D. R. Daughton, A. R. Arehart, S. A. Ringel, S. Rajan, and H. Zhao, Phys. Status Solidi RRL 2000145 (2020). DOI: 10.1002/pssr.202000145
- <sup>38</sup>S. Rafique, L. Han, and H. Zhao, Phys. Status Solidi A **213**, 1002 (2016).
- <sup>39</sup>S. Rafique, L. Han, M. J. Tadjer, J. A. Freitas Jr, N. A. Mahadik, and H. Zhao, Appl. Phys. Lett. 108, 182105 (2016).
- <sup>40</sup>S. Rafique, L. Han, A. T. Neal, S. Mou, M. J. Tadjer, R. H. French, and H. Zhao, Appl. Phys. Lett. 109, 132103 (2016).
- <sup>41</sup>S. Rafique, M. R. Karim, J. M. Johnson, J. Hwang, and H. Zhao, Appl. Phys. Lett. **112**, 052104 (2018).
- <sup>42</sup>A F M A. U. Bhuiyan, Z. Feng, J. M. Johnson, Z. Chen, H.-L. Huang, J. Hwang, and H. Zhao, Appl. Phys. Lett. **115**, 120602 (2019).
- <sup>43</sup>P. Ranga, A. Rishinaramangalam, J. Varley, A. Bhattacharyya, D. Feezell, and S. Krishnamoorthy, Appl. Phys. Express 12, 111004 (2019).
- <sup>44</sup>Z. Feng, M. R. Karim, and H. Zhao, APL Mater. 7, 022514 (2019).
- <sup>45</sup>M. R. Karim, Z. Feng, and H. Zhao, Cryst. Growth Des. **18**, 4495 (2018).
- <sup>46</sup>Y. Zhang, M. R. Karim, Z. Feng, and H. Zhao, J. Appl. Phys. **125**, 135703 (2019).
- <sup>47</sup>M. R. Karim, Z. Feng, J. M. Johnson, M. Zhu, J. Hwang, and H. Zhao, Cryst. Growth Des. 19, 1965 (2019).
- <sup>48</sup>P. Kisliuk, J. Phys. Chem. Solids **3**, 95 (1957).
- <sup>49</sup>T. Jin, V. García-López, S. Kuwahara, P. T. Chiang, J. M. Tour, and G. Wang, J. Phys. Chem. C 122, 19025 (2018).
- <sup>50</sup>T. Kimoto, and H. Matsunami, J. Appl. Phys. **78**, 3132 (1995).
- <sup>51</sup>W. K. Burton, N. Cabrera and F. C. Frank, Philos. Trans. R. Soc. A **243**, 299 (1951).
- <sup>52</sup>M. López, and Y. Nomura, J. Cryst. Growth. **150**, 68 (1995).
- <sup>53</sup>Y. Nomura, Y. Morishita, S. Goto, Y. Katayama, and T. Isu, Appl. Phys. Lett. **64**, 1123 (1994).

- <sup>54</sup>R. F. Xiao, and N. B. Ming, Phys. Rev. E **49**, 4720 (1994).
- <sup>55</sup>T. Bauer, M. Schreck, and B. Stritzker, Diam. Relat. Mater. **15**, 472 (2006).
- <sup>56</sup>J. H. Leach, K. Udwary, J. Rumsey, G. Dodson, H. Splawn, and K. R. Evans, APL MATER. 7, 022504 (2019).
- <sup>57</sup>S. B. Anooz, R. Grüneberg, C. Wouters, R. Schewski, M. Albrecht, A. Fiedler, K. Irmscher, Z. Galazka, W. Miller, G. Wagner, J. Schwarzkopf, and A. Popp, Appl. Phys. Lett. 116, 182106 (2020).